Journal of Computational Physics 467 (2022) 111463

Contents lists available at ScienceDirect

Journal of Computational Physics

www.elsevier.com/locate/jcp

A unified surface-gradient and hydrostatic reconstruction scheme for the shallow water equations

Guoxian Chen [a,b,*], Sebastian Noelle [c]

[a] School of Mathematics and Statistics, Wuhan University, Wuhan, 430072, PR China
[b] Computational Science Hubei Key Laboratory, Wuhan University, Wuhan, 430072, PR China
[c] Institute for Geometry and Practical Mathematics, RWTH Aachen University, Templergraben 55, 52062, Aachen, Germany

ARTICLE INFO

Article history:
Received 9 July 2021
Received in revised form 25 April 2022
Accepted 5 July 2022
Available online 13 July 2022

Keywords:
Saint-Venant system
Well-balanced property
Positivity preserving property
Subcell hydrostatic reconstruction
Bottom-surface-gradient method
Maximum-minimum property

ABSTRACT

We propose a new second-order accurate hydrostatic reconstruction scheme for the Saint-Venant system. Such a scheme needs to overcome several difficulties: besides the well-known issues of positivity and well-balancing there is also the difficulty of unphysical reflections from non-monotone bottom reconstructions. We address all of these problems at once by changing the logic of the reconstruction of the bottom, the water depth and the water surface level. The scheme gives excellent results in one and two space dimensions. To highlight the novel reconstruction of bottom and water surface, we call the scheme *bottom-surface-gradient method* (BSGM).

1. Introduction

The shallow water equations model incompressible free surface flow between a time independent, piecewise continuous bottom topography $z = b(x, y)$ and the water surface $z = w(x, y, t)$. The water height

$$h(x, y, t) := w(x, y, t) - b(x, y) \tag{1.1}$$

is assumed to be non-negative. The equations of motion are derived by depth-averaging the incompressible Euler equations, assuming uniform density of the water, kinematic boundary conditions at surface and bottom, hydrostatic pressure, and constant vertical velocity profiles [1,2]. They are given by

$$\partial_t h + \partial_x(hu) + \partial_y(hv) = 0 \tag{1.2}$$

$$\partial_t(hu) + \partial_x(hu^2 + \frac{1}{2}gh^2) + \partial_y(huv) = -gh\partial_x b \tag{1.3}$$

$$\partial_t(hv) + \partial_x(huv) + \partial_y(hv^2 + \frac{1}{2}gh^2) = -gh\partial_y b. \tag{1.4}$$

Here g is the gravitational constant, and $u(x, y, t)$ and $v(x, y, t)$ are the depth-averaged horizontal velocities, which are assumed to vanish in dry areas,

* Corresponding author.
E-mail addresses: gxchen.math@whu.edu.cn (G. Chen), noelle@igpm.rwth-aachen.de (S. Noelle).

https://doi.org/10.1016/j.jcp.2022.111463
0021-9991/

Table 1
Cartoon of the history of piecewise linear reconstructions of the vertical variables (b, h, w) for second-order finite volume schemes for the shallow water equations. $FV2_{adhoc}$: standard second-order non-well-balanced scheme based on a given reconstruction of b. $FV2_{ZCMI}$: the surface-gradient method by Zhou et al. [6], also based on a given reconstruction of b. $HR2_{ABBKP}$: the second-order version of the hydrostatic reconstruction method by Audusse et al. [9]. $HR2_{BHNW}$: modification due to Buttinger et al. $HR2_{CN}$: the present bottom-surface-gradient method. The three last columns indicate if the method is well-balanced, positivity preserving, and free of unphysical reflections due to non-monotone reconstructions of the bottom topography.

method	reconstructed	derived	well-balanced	positive	non-reflecting
$FV2_{adhoc}$	h	w:=b+h	no	yes	yes
$FV2_{ZCMI}$ = SGM	w	h:=w-b	yes	no	yes
$HR2_{ABBKP}$	(h, w)	b:=w-h	yes	yes	no
$HR2_{BHNW}$	(h, w) or (h, b)	(b:=w-h) or (w:=b+h)	yes	yes	sometimes
$HR2_{CN}$ = BSGM	w or $(w\,\&\,b)$	h:=w-b	yes	yes	yes

$$u(x, y, t) = v(x, y, t) = 0 \quad \text{if } h(x, y, t) = 0. \tag{1.5}$$

The left-hand-side of the equations is in divergence form and governs conservation of mass and momentum, and the right hand side is a non-conservative gravitational acceleration in case the bottom is inclined. The shallow water equations are widely used to model free surface flows such as rivers, lakes and oceans. Besides the many applications, the shallow water equations are a prototype of balance laws whose source term is a non-conservative product of measures, and is often singular.

There is a large amount of literature on finite-volume (FV) and discontinuous Galerkin (DG) schemes for the shallow water equations, among them virtually all papers cited in the bibliography [3–24], as well as the references given in the monographs [25–27] and the review article [28]. FV and DG schemes approximate the solution by piecewise polynomial functions, which are reconstructed and evolved in time.

Let us briefly review the underlying first-order accurate schemes in the context of singular source terms. These occur if either the physical topography or its numerical approximation are discontinuous at a cell interface. In this case the gradient of the bottom is a Dirac measure, which is multiplied by a discontinuous height [29]. The evaluation of this non-conservative product is not unique, and additional modelling assumptions are needed [29,30]. One of the most prominent choices is the hydrostatic reconstruction [9] together with its modification [20] introduced by the authors. We call these first-order hydrostatic reconstruction schemes $HR1_{ABBKP}$ and $HR1_{CN}$ (HR1 for first-order hydrostatic reconstruction scheme, and the subscript for the author's initials).

The evaluation of the singular source term via hydrostatic reconstruction as in [9,20] can be used directly as a building block of higher order finite volume schemes. In the present manuscript we take the hydrostatic reconstruction for granted and do not discuss it further. Extensive numerical comparisons of several first order hydrostatic reconstruction schemes may be found in [20].

Here we focus on second-order accurate finite volume schemes based on piecewise linear approximations. For the shallow water equations, the situation is not understood as well, since there are three variables related to the vertical space dimension, only two of which are independent:

$$b(x, y), \quad w(x, y, t) \quad \text{and} \quad h(x, y, t) := w(x, y, t) - b(x, y). \tag{1.6}$$

We study how the three criteria of well-balancing, positivity, and monotonicity of the bottom topography can be met by reconstructing just two of the vertical variable (b, h, w). Many authors have addressed this issue. We list the schemes discussed in this paper together with some of their properties in Table 1.

In one family of schemes, the bottom topography is a prescribed continuous, piecewise linear function [6,7]. In an ad-hoc approach, the water depth h would be reconstructed, leading to possible loss of well-balancing. If the surface w is reconstructed, the lake-at-rest is preserved, but it requires extra work to guarantee positivity, see e.g. [7,13,19]. Another family of schemes, due to Audusse et al. [9], reconstructs surface and depth (and hence preserves the lake-at-rest and guarantees positive water height). This introduces a piecewise linear approximation of the bottom, with

$$\nabla b(t) := \nabla w(t) - \nabla h(t). \tag{1.7}$$

The gradient of b is constant in each cell, but varies with time. Buttinger et al. [31] observed that non-monotone piecewise linear reconstructions of the bottom may lead to unphysical reflections of waves, and gave a cure for this problem in several cases.

The bottom-surface-gradient method (BSGM or $HR2_{CN}$) presented in this paper unifies the SGM (or $FV2_{ZCMI}$) and the classical second order hydrostatic reconstruction method $HR2_{ABBKP}$. Starting from an initially prescribed piecewise linear, continuous or discontinuous bottom approximation, we first compute a preliminary reconstruction of the water surface level w. As in the SGM, it may happen that the reconstructed piecewise linear w together with the initially prescribed approximation of b produce negative water height $h := w - b$. Note that these cells will contain a wet-dry front. Reconstructing these fronts within the interior of the computational cells leads to rather complex algorithms [19,22]. Here we

propose a simpler way to guarantee non-negative water height by correcting the slopes of surface and bottom simultaneously (as indicated by ($w\,\&\,b$) in Table 1), and moving the wet-dry front to a cell interface. The correction satisfies the MMP (minimum-maximum-preserving) property in b and w. The resulting scheme is well-balanced, positivity-preserving, and due to the MMP property it creates no unphysical reflections. It is simple and efficient, can be extended dimension by dimension to two-dimensional cartesian grids, and gives excellent computational results.

The paper is organized as follows: In Section 2, we introduce the bottom-surface gradient reconstruction. In Section 3 we define the finite volume update, including the hydrostatic reconstruction and the computation of the singular source terms. In Section 4 we establish the positivity and well-balancing properties in one space dimension. The two-dimensional extension is given in Section 5. In Section 6, we present numerical experiments which demonstrate second-order accuracy, well-balancing and positivity. We compute several one-dimensional Riemann problems and two-dimensional dambreak problems for which state-of-the art schemes may produce unphysical reflections. These demonstrate the quality of the BSGM.

2. Piecewise linear reconstruction

Let $\Omega \subset \mathbb{R}$ be a one-dimensional domain, and let $b : \Omega \to \mathbb{R}$ be the given topography. Discretize the domain as $\Omega = \bigcup_{i\in I} C_i$ with cells $C_i := (x_{i-\frac{1}{2}}, x_{i+\frac{1}{2}})$ and an index set $I \subset \mathbb{Z}$. For simplicity, we choose a uniform grid with $x_{i+\frac{1}{2}} - x_{i-\frac{1}{2}} = \Delta x$. Let $h_i = h_i(t)$, $(hu)_i = (hu)_i(t)$ and $(hv)_i = (hv)_i(t)$ be the computed cell averages of the conserved variables, and let $w_i = w_i(t) = h_i(t) + b_i$ be the corresponding surface levels. Note that we compute the initial cell averages using the midpoint rule, which helps to recover a discrete lake-at-rest initial data (Definition 4.2) for the wet-dry cells if the lake is at rest (Definition 4.1). We introduce index sets for the wet and dry regions,

$$I_{wet}(t) := \{i \in I \mid h_i > 0\}, \qquad I_{dry}(t) := \{i \in I \mid h_i = 0\}. \tag{2.1}$$

Then we distinguish between those cells which are adjacent to the wet-dry front, and those which are in the interior of the respective regions:

$$I^{front}_{wet}(t) := \{i \in I_{wet}(t) \mid \min(h_{i\pm1}) = 0\}, \qquad I^{int}_{wet}(t) := I_{wet}(t) \setminus I^{front}_{wet}(t), \tag{2.2}$$

$$I^{front}_{dry}(t) := \{i \in I_{dry}(t) \mid \max(h_{i\pm1}) > 0\}, \qquad I^{int}_{dry}(t) := I_{dry}(t) \setminus I^{front}_{dry}(t), \tag{2.3}$$

so $I_{wet}(t) = I^{front}_{wet}(t) \cup I^{int}_{wet}(t)$ and $I_{dry}(t) = I^{front}_{dry}(t) \cup I^{int}_{dry}(t)$. In the following, we construct preliminary piecewise linear approximations of h, w, u and v, and if this produces negative water heights, we correct the slopes of w and b.

2.1. Initial approximation of the bottom

Once and for all, let $b^{\#}(x)$ be the prescribed initial, piecewise linear, possibly discontinuous reconstruction of a given topography. In exceptional cases, when the cell contains a wet-dry front, the initial bottom reconstruction will be replaced by a modified reconstruction $b^{\#\#}(x)$, see Section 2.3. The important case that $b^{\#}(x)$ may be continuous in smooth parts of the topography is discussed in Remark 3.1 below.

2.2. Preliminary reconstruction of the flow variables

Define the velocities by

$$(u_i, v_i) := \begin{cases} \left(\frac{(hu)_i}{h_i}, \frac{(hv)_i}{h_i}\right) & \text{if } h_i > \varepsilon, \\ (0,0) & \text{otherwise,} \end{cases} \tag{2.4}$$

where ε is a small a-priori chosen positive number to avoid the division by very small numbers. In this paper, we choose $\varepsilon = 1.0 \times 10^{-10}$.

For any scalar quantity $q \in \{w, u, v\}$, we define a preliminary, discontinuous, piecewise linear reconstruction by

$$q^{\#}(x,t) := q_i(t) + (x - x_i)\,\partial^{\#}_x q_i(t) \quad \text{for } x \in C_i, \tag{2.5}$$

where $\partial^{\#}_x q_i$ is an approximate slope of q in the cell. If $i \in I^{int}_{dry}(t)$ we simply set

$$\partial^{\#}_x u_i = \partial^{\#}_x v_i = 0, \quad \partial^{\#}_x w_i = \partial^{\#}_x b_i. \tag{2.6}$$

Otherwise if $i \in I_{wet}(t) \cup I^{front}_{dry}(t)$, we compute the slope using a standard limiter function. We choose

$$\partial^{\#}_x q_i := \operatorname{minmod}\left(\theta \frac{q_i - q_{i-1}}{\Delta x}, \frac{q_{i+1} - q_{i-1}}{2\Delta x}, \theta \frac{q_{i+1} - q_i}{\Delta x}\right), \tag{2.7}$$

with minmod function

$$\operatorname{minmod}(a_1, a_2, \cdots, a_m) := \begin{cases} \max\limits_i a_i, & \text{if } \max\limits_i a_i < 0, \\ \min\limits_i a_i, & \text{if } \min\limits_i a_i > 0, \\ 0, & \text{otherwise.} \end{cases} \tag{2.8}$$

The parameter $\theta \in [1, 2]$ controls the numerical viscosity of the numerical scheme. We set $\theta := 1.3$. Finally, we define the preliminary height by

$$h^{\#}(x, t) := w^{\#}(x, t) - b^{\#}(x, t). \tag{2.9}$$

For future reference we also introduce the one-sided limits

$$q^l_{i+\frac{1}{2}}(t) := q^{\#}(x_{i+\frac{1}{2}} - 0, t), \tag{2.10}$$

$$q^r_{i+\frac{1}{2}}(t) := q^{\#}(x_{i+\frac{1}{2}} + 0, t) \tag{2.11}$$

for $q \in \{h, u, v, w\}$.

2.3. Corrected reconstruction

In this section we correct the piecewise linear reconstruction in wet-dry cells, which are identified by

$$I^{\#}_{wetdry}(t) = \left\{ i \in I |\ \min_{x \in C_i} h^{\#}(x, t) < 0 < \max_{x \in C_i} h^{\#}(x, t) \right\}. \tag{2.12}$$

Note that $I^{\#}_{wetdry}(t) \subset I_{wet}(t) \cup I^{front}_{dry}(t)$, since $h^{\#}$ vanishes identically in $I^{int}_{dry}(t)$. It would be interesting to see if $I^{\#}_{wetdry}(t) \subset I^{front}_{wet}(t) \cup I^{front}_{dry}(t)$, i.e. if wet-dry cells could also occur in the interior $I^{int}_{wet}(t)$ of wet regions.

Let $i \in I^{\#}_{wetdry}(t)$. Since the minimum of $h^{\#}(\cdot, t)$ lies at one of the endpoints $x_{i\pm 1/2}$, we distinguish two cases:

- If $w^r_{i-\frac{1}{2}}(t) < b^r_{i-\frac{1}{2}}(t)$, we call the left interface $(i - \frac{1}{2})$ a *wet-dry front at time t* and set

$$z_{i-\frac{1}{2}+}(t) := w_i(t) + \operatorname{minmod}(w^r_{i-\frac{1}{2}}(t) - w_i(t), b^r_{i-\frac{1}{2}}(t) - w_i(t)). \tag{2.13}$$

  For $q \in \{b, w\}$ we redefine the slopes by

$$\partial^{\#\#}_x q_i(t) := \frac{q_i(t) - z_{i-\frac{1}{2}+}(t)}{\Delta x/2}. \tag{2.14}$$

- If $w^l_{i+\frac{1}{2}}(t) < b^l_{i+\frac{1}{2}}(t)$, we call the right interface $(i + \frac{1}{2})$ a *wet-dry front at time t* and set

$$z_{i+\frac{1}{2}-}(t) := w_i(t) + \operatorname{minmod}(w^l_{i+\frac{1}{2}}(t) - w_i(t), b^l_{i+\frac{1}{2}}(t) - w_i(t)). \tag{2.15}$$

  For $q \in \{b, w\}$ we redefine the slopes by

$$\partial^{\#\#}_x q_i(t) = \frac{z_{i+\frac{1}{2}-}(t) - q_i(t)}{\Delta x/2}. \tag{2.16}$$

Once more, let $q \in \{b, w\}$. Given the modified slopes $\partial^{\#\#}_x q_i(t)$, the corrected reconstruction is

$$q^{\#\#}_i(x, t) := \begin{cases} q_i(t) + (x - x_i)\partial^{\#\#}_x q_i(t) & \text{if } i \in I^{\#}_{wetdry}(t), \\ q^{\#}(x, t) & \text{otherwise.} \end{cases} \tag{2.17}$$

The corrected reconstructions of h, u and v are given by

$$h^{\#\#}(x, t) := w^{\#\#}(x, t) - b^{\#\#}(x, t) \tag{2.18}$$

$$u^{\#\#}(x, t) := u^{\#}(x, t), \tag{2.19}$$

$$v^{\#\#}(x, t) := v^{\#}(x, t). \tag{2.20}$$

For $q \in \{b, h, u, v, w\}$, we denote the one-sided limits of the corrected reconstruction by

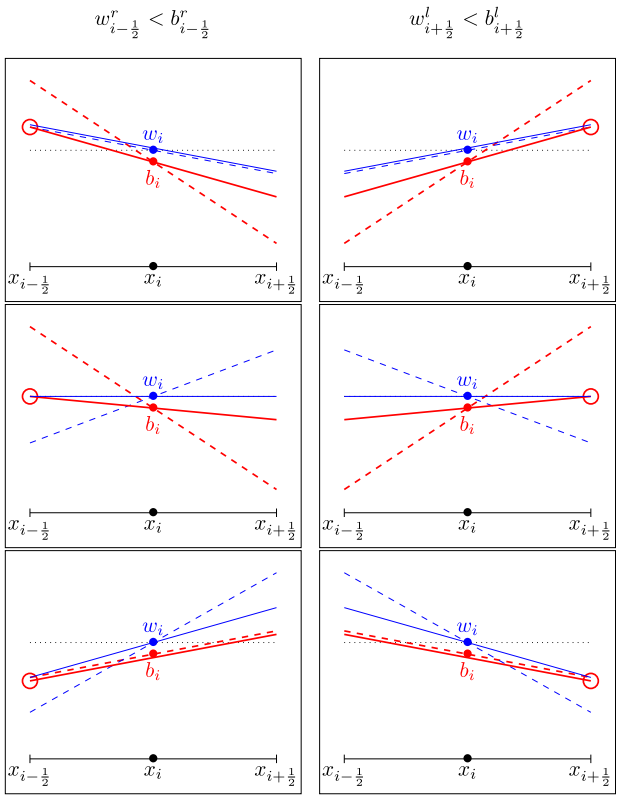

Fig. 1. The BSGM reconstruction for a cell C_i which is wet-dry at time t. Left column: interface $(i-\frac{1}{2})$ is wet-dry at time t. Right column: interface $(i+\frac{1}{2})$ is wet-dry at time t. Preliminary reconstruction: red dashed lines: $b_i^{\#}(x,t)$; blue dashed lines: $w_i^{\#}(x,t)$. Corrected reconstruction: red lines: $b_i^{\#\#}(x,t)$; blue lines: $w_i^{\#\#}(x,t)$. Upper row: only $\partial_x^{\#} b$ is limited. Centre row: both $\partial_x^{\#} b$ and $\partial_x^{\#} w$ are limited. Lower row: only $\partial_x^{\#} w$ is limited. The interface levels $z_{i-\frac{1}{2}+}$ and $z_{i+\frac{1}{2}-}$ are marked by red circles. (For interpretation of the colours in the figure(s), the reader is referred to the web version of this article.)

$$q_{i+\frac{1}{2}-}(t) := q^{\#\#}(x_{i+\frac{1}{2}} - 0, t), \tag{2.21}$$

$$q_{i+\frac{1}{2}+}(t) := q^{\#\#}(x_{i+\frac{1}{2}} + 0, t). \tag{2.22}$$

Please note the subtle difference with the notation for the edge values $q^{l/r}_{i\pm\frac{1}{2}}(t)$ of the preliminary reconstruction $q^{\#}(x,t)$, see (2.10), (2.11)).

Remark 2.1. (i) We call (2.17) - (2.19) the bottom-surface-gradient (BSGM) reconstruction.
(ii) Fig. 1 shows the details of the BSGM correction for bottom and surface in a wet-dry cell.

2.4. Stability properties of the BSGM-reconstruction

The BSGM reconstruction satisfies the following monotonicity properties:

Theorem 2.2. *At the left interface of cell C_i,*

$$h_{i-\frac{1}{2}+} \geq 0 \qquad \text{for all } i \in I, \tag{2.23}$$

$$\min(w_{i-1}, w_i) \leq w_{i-\frac{1}{2}+} \leq \max(w_{i-1}, w_i) \qquad \text{for all } i \in I_{wet}(t) \cup I^{front}_{dry}(t) \tag{2.24}$$

$$\min(b^r_{i-\frac{1}{2}}, b_i) \leq b_{i-\frac{1}{2}+} \leq \max(b^r_{i-\frac{1}{2}}, b_i) \qquad \text{for all } i \in I^{\#}_{wetdry}(t) \tag{2.25}$$

and analogously at the right interface,

$$h_{i+\frac{1}{2}-} \geq 0 \qquad \text{for all } i \in I, \tag{2.26}$$

$$\min(w_i, w_{i+1}) \leq w_{i+\frac{1}{2}-} \leq \max(w_i, w_{i+1}) \qquad \text{for all } i \in I_{wet}(t) \cup I^{front}_{dry}(t) \tag{2.27}$$

$$\min(b_i, b^l_{i+\frac{1}{2}}) \le b_{i+\frac{1}{2}-} \le \max(b_i, b^l_{i+\frac{1}{2}}) \qquad \text{for all } i \in I^{\#}_{wetdry}(t). \tag{2.28}$$

Remark 2.3 *(MMP property of the bottom reconstruction).* Theorem 2.2 lays the basis for the stability analysis of the BSGM scheme in Section 4. In particular, (2.25) and (2.28) mean that the corrected reconstruction of the bottom in wet-dry cells, $b^{\#\#}(x,t)$, is maximum-minimum-preserving (MMP). This is in contrast with previous HR schemes [9,20], and our numerical experiments indicate that this helps to avoid unphysical reflected waves in the numerical solution.

Proof. By the monotonicity of the minmod function (2.8), we have that after the preliminary reconstruction

$$\min(w_{i-1}, w_i) \le w^r_{i-\frac{1}{2}} \le \max(w_{i-1}, w_i), \tag{2.29a}$$

$$\min(w_i, w_{i+1}) \le w^l_{i+\frac{1}{2}} \le \max(w_i, w_{i+1}). \tag{2.29b}$$

Thus the sufficient conditions for (2.24) and (2.27) are

$$\min(w^r_{i-\frac{1}{2}}, w_i) \le w_{i-\frac{1}{2}+} \le \max(w^r_{i-\frac{1}{2}}, w_i) \tag{2.30a}$$

$$\min(w_i, w^l_{i+\frac{1}{2}}) \le w_{i+\frac{1}{2}-} \le \max(w_i, w^l_{i+\frac{1}{2}}), \tag{2.30b}$$

By the linearity of both $w^{\#}_i(x)$ and $w^{\#\#}_i(x)$ in cell I_i, we know that (2.30a) and (2.30b) are equivalent. Similarly we get the equivalence between (2.25) and (2.28). These tell us that we only need to prove (2.30a), (2.25) or (2.30b), (2.28).

We next move to effect of corrected reconstruction step. Let $i \in I^{\#}_{wetdry}(t)$ in where the correction step is activated.

Without losing generality we first consider the case that the right interface $(i+\frac{1}{2})$ is a wet-dry front at time t, i.e. $w^l_{i+\frac{1}{2}} < b^l_{i+\frac{1}{2}}$. Notice that the reconstructed surface level and bottom at $x_{i+\frac{1}{2}}$ in cell I_i share the same value $w_{i+\frac{1}{2}-} = b_{i+\frac{1}{2}-} = z_{i+\frac{1}{2}-}$ with the new freedom $z_{i+\frac{1}{2}-}$ defined by (2.13). Thus (2.30b), (2.28) are equivalent to the following inequalities

$$\min(w_i, w^l_{i+\frac{1}{2}}) \le z_{i+\frac{1}{2}-} \le \max(w_i, w^l_{i+\frac{1}{2}}), \quad \min(b_i, b^l_{i+\frac{1}{2}}) \le z_{i+\frac{1}{2}-} \le \max(b_i, b^l_{i+\frac{1}{2}}). \tag{2.31}$$

By the property of the minmod function (2.8), the value of $z_{i+\frac{1}{2}-}$ dependent on the three quantities $w^l_{i+\frac{1}{2}}$, $b^l_{i+\frac{1}{2}}$ and w_i by

$$z_{i+\frac{1}{2}-} = \begin{cases} w^l_{i+\frac{1}{2}}, & w_i \le w^l_{i+\frac{1}{2}} < b^l_{i+\frac{1}{2}} \\ w_i, & w^l_{i+\frac{1}{2}} \le w_i \le b^l_{i+\frac{1}{2}} \\ b^l_{i+\frac{1}{2}}, & w^l_{i+\frac{1}{2}} < b^l_{i+\frac{1}{2}} \le w_i \end{cases} \tag{2.32}$$

which means that $z_{i+\frac{1}{2}-}$ choose the value of w_i if $w^l_{i+\frac{1}{2}}$ and $b^l_{i+\frac{1}{2}}$ are located at different sides of w_i; otherwise choose the closer one in $w^l_{i+\frac{1}{2}}$ and $b^l_{i+\frac{1}{2}}$ from w_i (see also from the Fig. 1). It is checked from above equation that the value of $z_{i+\frac{1}{2}-}$ satisfies the relation (2.31). Then (2.30b), (2.28) and further ((2.24), (2.27), (2.25)) and (2.28) hold.

The positivity (2.23) and (2.26) comes from the fact $b_{i+\frac{1}{2}-} = w_{i+\frac{1}{2}-} = z_{i+\frac{1}{2}-}$ which deduces that $h_{i+\frac{1}{2}-} = 0$ and then $h_{i-\frac{1}{2}+} = 2h_i - h_{i+\frac{1}{2}-} = 2h_i$ for cell $i \in I^{\#}_{wetdry}(t)$.

If the left interface $(i+\frac{1}{2})$ is a wet-dry front at time t, i.e. $w^r_{i-\frac{1}{2}} < b^r_{i-\frac{1}{2}}$. Analogously we can prove (2.30a), (2.25) then ((2.24), (2.27), (2.25)) and (2.28). The positivity (2.23) and (2.26) is that $h^r_{i-\frac{1}{2}} = 0$ and $h_{i+\frac{1}{2}-} = 2h_i$ for cell $i \in I^{\#}_{wetdry}(t)$.

This concludes the proof. □

3. Finite volume update in 1D

In this section we suppose that the corrected reconstructions $q^{\#\#}(x,t)$ are already constructed, and, in particular, the corrected one-sided limits $q_{i+\frac{1}{2}\pm}$ are given by (2.21) - (2.22).

We rewrite the one-dimensional shallow water equations as

$$\partial_t U + \partial_x F(U) = S(U,x), \tag{3.1}$$

with

$$U := \begin{pmatrix} h \\ hu \\ hv \end{pmatrix}, \quad F(U) := \begin{pmatrix} hu \\ hu^2 + \frac{1}{2}gh^2 \\ huv \end{pmatrix} \quad \text{and} \quad S(U,x) := -\begin{pmatrix} 0 \\ gh\partial_x b(x) \\ 0 \end{pmatrix}. \tag{3.2}$$

As in [20], we start with a semi-discrete method of lines for the cell averages $U_i(t)$,

$$\frac{d}{dt}U_i(t) = R_i(t) := -\frac{1}{\Delta x}\left(F_{i+\frac{1}{2}} - F_{i-\frac{1}{2}}\right) + S_{i-\frac{1}{2}+} + S_i + S_{i+\frac{1}{2}-} \tag{3.3}$$

Based on the reconstruction of the previous section, we compute the central source term as

$$S_i := \left(0, -g\,\frac{h_{i-\frac{1}{2}+} + h_{i+\frac{1}{2}-}}{2}\,\frac{b_{i+\frac{1}{2}-} - b_{i-\frac{1}{2}+}}{\Delta x}, 0\right)^T. \tag{3.4}$$

If $b_{i+\frac{1}{2}-} = b_{i+\frac{1}{2}+}$, then the singular source terms $S_{i+\frac{1}{2}\pm}$ vanish. If the bottom is discontinuous (either because of the initial data or because of the BSGM correction (2.14) (2.16)), then we compute hydrostatic reconstruction values $b^\star_{i+\frac{1}{2}}, U^\star_{i+\frac{1}{2}\pm}$ as in [20, (2.15)-(2.16)]:

$$b^\star_{i+\frac{1}{2}} := \min(w_{i+\frac{1}{2}-}, w_{i+\frac{1}{2}+}, \max(b_{i+\frac{1}{2}-}, b_{i+\frac{1}{2}+})), \tag{3.5}$$

$$h^\star_{i+\frac{1}{2}-} := \min(w_{i+\frac{1}{2}-} - b^\star_{i+\frac{1}{2}}, h_{i+\frac{1}{2}-}), \tag{3.6}$$

$$h^\star_{i+\frac{1}{2}+} := \min(w_{i+\frac{1}{2}+} - b^\star_{i+\frac{1}{2}}, h_{i+\frac{1}{2}+}), \tag{3.7}$$

$$(hu)^\star_{i+\frac{1}{2}\pm} := h^\star_{i+\frac{1}{2}\pm}\, u_{i+\frac{1}{2}\pm}, \tag{3.8}$$

$$(hv)^\star_{i+\frac{1}{2}\pm} := h^\star_{i+\frac{1}{2}\pm}\, v_{i+\frac{1}{2}\pm}. \tag{3.9}$$

Note that this also defines the vectors $U^\star_{i+\frac{1}{2}\pm}$. Then we evaluate the singular source terms following [20, (2.17)-(2.18)]:

$$s_{i+\frac{1}{2}-} := -g\,\frac{h_{i+\frac{1}{2}-} + h^\star_{i+\frac{1}{2}-}}{2}\,\frac{b^\star_{i+\frac{1}{2}} - b_{i+\frac{1}{2}-}}{\Delta x}, \tag{3.10}$$

$$s_{i+\frac{1}{2}+} := -g\,\frac{h_{i+\frac{1}{2}+} + h^\star_{i+\frac{1}{2}-}}{2}\,\frac{b_{i+\frac{1}{2}+} - b^\star_{i+\frac{1}{2}}}{\Delta x}, \tag{3.11}$$

and set

$$S_{i+\frac{1}{2}\pm} := (0, s_{i+\frac{1}{2}\pm}, 0)^T. \tag{3.12}$$

Finally, we compute the numerical flux evaluating the Harten-Lax-Van Leer Riemann solver at the hydrostatic values,

$$F_{i+\frac{1}{2}} := \mathcal{F}_{\mathrm{HLL}}(U^*_{i+\frac{1}{2}-}, U^*_{i+\frac{1}{2}+}). \tag{3.13}$$

Plugging (3.4), (3.12) and (3.13) into (4.19) determines the semi-discrete update.

Remark 3.1. Note that the corrected topography $b^{\#\#}(x)$ may be continuous across the cell interface, $b_{i+\frac{1}{2}-} = b_{i+\frac{1}{2}+}$ for the values defined in (2.21) - (2.22). In this case the singular source terms vanish, and (3.12), (3.13) may be replaced by

$$S_{i+\frac{1}{2}\pm} = 0, \quad F_{i+\frac{1}{2}} := \mathcal{F}_{\mathrm{HLL}}(U_{i+\frac{1}{2}-}, U_{i+\frac{1}{2}+}). \tag{3.14}$$

This may enhance the efficiency of the code.

The fully-discrete update is computed by applying Heun's second-order accurate SSP Runge-Kutta method [32] to the semi-discrete system (4.19).

4. Positivity and well-balancing in 1D

To capture the wet-dry front more precisely, we re-define

Definition 4.1 *(lake-at-rest).* The solution of the shallow water equations is at rest if for all $t \in [0, T]$

$$u(x,t) = v(x,t) = 0 \quad \text{for } x \in \Omega \tag{4.1}$$

$$\partial_x w(x,t) = 0 \quad \text{for } x \in \Omega_{wet}(t), \tag{4.2}$$

$$\lim_{\substack{x \to x_F \\ x \in \Omega_{wet}(t)}} w(x,t) \le \max\Big(\lim_{\substack{x \to x_F \\ x \in \Omega_{dry}(t)}} b(x), \lim_{\substack{x \to x_F \\ x \in \Omega_{wet}(t)}} b(x) \Big) \quad \text{for } x_F \in \Gamma(t) \tag{4.3}$$

where $\Omega_{wet}(t) := \{x |\, b(x) < w(x,t)\}$ and $\Omega_{dry}(t) := \{x |\, b(x) = w(x,t)\}$ are the wet and dry subdomains at time t (determined by a given solution $h(x,t)$), and $\Gamma(t)$ is the wet-dry front.

Condition (4.3) means that at the wet-dry front, the dry bottom should be at least as high as the adjacent water surface, and hence it prevents water from flowing out of the wet region.

Now we define a discrete lake-at-rest state:

Definition 4.2 *(discrete lake-at-rest).* We say that an approximate solution U_i^n satisfies the *discrete lake-at-rest condition* if the velocity vanishes everywhere,

$$u_i = v_i = 0 \quad \text{for all } i \in I, \tag{4.4}$$

the water surface level is constant in the interior of the wet region,

$$w_i = w_j \quad \text{for } i, j \in I_{wet}(t) \text{ and } |i - j| = 1 \tag{4.5}$$

and at the wet side of the front

$$w_i \le b_j, \quad \text{for } i \in I_{wet}^{front}(t) \text{ and } j \in \{i \pm 1\} \cap I_{dry}(t). \tag{4.6}$$

The discrete wet and dry domains where introduce at the beginning of Section 2.

Theorem 4.3. *Under the assumption that*

$$\frac{\Delta t}{\Delta x} \max(|u^n_{i+\frac{1}{2}\pm}| + \sqrt{g h^n_{i+\frac{1}{2}\pm}}) \le \frac{1}{2}, \tag{4.7}$$

the scheme is positivity preserving, i.e. $h_i^{n+1} \ge 0$.

Proof. By (2.23) and (2.26), we have the positivity of the reconstructed water height $h_{i+\frac{1}{2}\pm} \ge 0$ at every cell interface. The subcell hydrostatic reconstruction (3.5) gives

$$0 \le h^\star_{i-\frac{1}{2}+} \le h_{i-\frac{1}{2}+}, \;\; 0 \le h^\star_{i+\frac{1}{2}-} \le h_{i+\frac{1}{2}-}. \tag{4.8}$$

Therefore

$$h_i = \frac{h_{i-\frac{1}{2}+} + h_{i+\frac{1}{2}-}}{2} \ge \frac{h^\star_{i-\frac{1}{2}+} + h^\star_{i+\frac{1}{2}-}}{2}. \tag{4.9}$$

Thus we have the lower bound estimation of the one step forward Euler method

$$\begin{aligned} h_i + \Delta t\, R_i^{(h)} &= h_i - \frac{\Delta t}{\Delta x}\left(F^{(1)}_{i+\frac{1}{2}} - \mathbf{F}^{(1)}_{i-\frac{1}{2}} \right) \\ &\ge \frac{1}{2}\left(h^\star_{i-\frac{1}{2}+} + \frac{2\Delta t}{\Delta x} \mathcal{F}^{(1)}_{\mathrm{HLL}}(U^\star_{i-\frac{1}{2}-}, U^\star_{i-\frac{1}{2}+}) \right) + \frac{1}{2}\left(h^\star_{i+\frac{1}{2}-} - \frac{2\Delta t}{\Delta x} \mathcal{F}^{(1)}_{\mathrm{HLL}}(U^\star_{i+\frac{1}{2}-}, U^\star_{i+\frac{1}{2}+}) \right) \\ &\ge 0, \end{aligned} \tag{4.10}$$

where we have used the positivity property of the HLL flux [33,26,19] and the CFL condition (4.7). Since Heun's Runge-Kutta method is a strong-stability preserving (see e.g. [32]), the final update is non-negative.

This concludes the proof. □

Theorem 4.4 *(well-balancing for the 1D lake-at-rest). If the data at time* $t = t^n$ *satisfy the discrete lake-at-rest condition, then* $R_i(t^n) = 0$ *for all cells, so the scheme is well-balanced.*

Proof. Suppose the data at time $t = t^n$ satisfy the discrete Lake-at-Rest conditions according to Definition 4.2. It follows by inspection that

$$u_{i\pm\frac{1}{2}-} = u_{i\pm\frac{1}{2}+} = v_{i\pm\frac{1}{2}-} = v_{i\pm\frac{1}{2}+} = 0 \qquad \text{for all } i \in I \tag{4.11}$$

$$h^\star_{i\pm\frac{1}{2}-} = h^\star_{i\pm\frac{1}{2}+} =: h^\star_{i\pm\frac{1}{2}} \qquad \text{for all } i \in I \tag{4.12}$$

$$w^\star_{i-\frac{1}{2}} = w_{i-\frac{1}{2}+} = w_{i+\frac{1}{2}-} = w^\star_{i+\frac{1}{2}} \qquad \text{for all } i \in I_{wet}(t). \tag{4.13}$$

In particular, if $i \in I_{dry}(t)$, $h^\star_{i\pm\frac{1}{2}} = 0$. Then $R_i = 0$. For $i \in I_{wet}(t)$,

$$U^\star_{i\pm\frac{1}{2}-} = U^\star_{i\pm\frac{1}{2}+} =: U^\star_{i\pm\frac{1}{2}} = (h^\star_{i\pm\frac{1}{2}}, 0, 0)^\top \tag{4.14}$$

$$F_{i\pm\frac{1}{2}} = F(U^\star_{i\pm\frac{1}{2}}) = \left(0, \frac{g}{2}(h^\star_{i\pm\frac{1}{2}})^2, 0\right)^\top. \tag{4.15}$$

Note that the first components of all residual terms vanish,

$$R^{(1)}_i = R^{(1)}_{i-\frac{1}{2}+} = R^{(1)}_{i+\frac{1}{2}-} = 0.$$

Using (4.13) we can rewrite the second components of the source terms as

$$\begin{aligned} S^{(2)}_i &= -g\,\frac{h_{i-\frac{1}{2}+} + h_{i+\frac{1}{2}-}}{2}\,\frac{(w_{i+\frac{1}{2}-} - h_{i+\frac{1}{2}-}) - (w_{i-\frac{1}{2}+} - h_{i-\frac{1}{2}+})}{\Delta x} \\ &= \frac{g}{2\Delta x}\left(\left(h_{i+\frac{1}{2}-}\right)^2 - \left(h_{i-\frac{1}{2}+}\right)^2\right) \\ &= \frac{1}{\Delta x}\left(F^{(2)}(U_{i+\frac{1}{2}-}) - F^{(2)}(U_{i-\frac{1}{2}+})\right), \end{aligned} \tag{4.16}$$

Similarly,

$$S^{(2)}_{i-\frac{1}{2}+} = \frac{1}{\Delta x}\left(F^{(2)}(U_{i-\frac{1}{2}+}) - F^{(2)}(U^\star_{i-\frac{1}{2}+})\right), \tag{4.17}$$

$$S^{(2)}_{i+\frac{1}{2}-} = \frac{1}{\Delta x}\left(F^{(2)}(U^\star_{i+\frac{1}{2}}) - F^{(2)}(U_{i+\frac{1}{2}-})\right). \tag{4.18}$$

Using (4.16) - (4.18) in (4.19) gives

$$\begin{aligned} R_i &= -\frac{1}{\Delta x}\left(F_{i+\frac{1}{2}} - F_{i-\frac{1}{2}}\right) + S_{i-\frac{1}{2}+} + S_i + S_{i+\frac{1}{2}-} \\ &= \frac{g}{2\Delta x}\Big(-F(U^\star_{i+\frac{1}{2}}) + F(U^\star_{i-\frac{1}{2}}) + F(U_{i-\frac{1}{2}+}) - F(U^\star_{i-\frac{1}{2}}) \\ &\qquad + F(U_{i+\frac{1}{2}-}) - F(U_{i-\frac{1}{2}+}) + F(U^\star_{i+\frac{1}{2}}) - F(U_{i+\frac{1}{2}-})\Big) \\ &= 0. \end{aligned} \tag{4.19}$$

This concludes the proof. □

5. Finite volume scheme in 2D

We extend the 1D hydrostatic reconstruction scheme dimension by dimension to the 2D case using rectangular grids. Analogously to the 1D case, let $b^\#(x, y)$ be the prescribed initial, piecewise linear, possibly discontinuous reconstruction of the given topography. The 1D preliminary and modified reconstructions of Section 2 are carried over without any changes to the y-direction. This yields a second-order accurate, positivity-preserving and well-balanced 2D solver.

6. Numerical experiments

In this section, we compare the second-order hydrostatic reconstruction schemes $\text{HR2}_{\text{ABBKP}}$, HR2_{BHNW} and HR2_{CN} (i.e. the BSGM scheme). All of them are well-balanced and positivity preserving. We do not include the second-order SGM scheme of Zhou et al., because it may produce negative water heights and would crash for several of our test problems.

In Example 6.1 we demonstrate second order accuracy for a smooth, two-dimensional solution. Example 6.2 shows well-balancing for a two-dimensional lake-at-rest solution and illustrates the activation of the BSGM correction at the wet-dry front. Section 6.3 shows various instances in 1D and 2D where unphysical wave-reflections due to non-monotonicity of the bottom reconstruction occur for the $\text{HR2}_{\text{ABBKP}}$ and HR2_{BHNW} schemes. This is cured by the BSGM scheme. The appendix provides details how we compute the reference for discontinuous bottom. In all examples, we use the gravitational constant $g = 9.812$.

Table 2
BSGM scheme: L^1-errors and experimental orders of convergence for Example 6.1.

# cells	h error	EOC	hu error	EOC	hv error	EOC
50 × 50	1.67e-3	-	4.06e-3	-	3.96e-3	-
100 × 100	4.26e-4	1.97	9.73e-4	2.06	9.43e-4	2.07
200 × 200	1.02e-4	2.05	2.27e-4	2.09	2.20e-4	2.10
400 × 400	2.54e-5	2.01	4.51e-5	2.33	4.55e-5	2.27

6.1. Accuracy

We test the accuracy for a smooth, very thin water film in the domain $[0, 1] \times [0, 1]$ with periodic boundary conditions. The bottom topography and initial values are

$$\begin{aligned} b(x, y) &= \tfrac{1}{2}(\sin^2(\pi x) + \cos^2(\pi y)), \\ h(x, y, 0) &= \tfrac{1}{2}\left(e^{\cos(2\pi x)} + e^{\sin(2\pi y)}\right) - e^{-1} + 0.00001, \\ u(x, y, 0) &= \sin(\cos(2\pi x)), \quad v(x, y, 0) = \cos(\sin(2\pi y)). \end{aligned} \tag{6.1}$$

Note that the minimal water height is 10^{-5}. We run the solution until final time $t = 0.04$, where it is still smooth. The reference solution is computed on 800×800 cells. The L^1-errors at final time are displayed in Table 2 and show second-order accuracy.

6.2. Well-balancing and positivity

Here we test the BSGM scheme for a two-dimensional lake-at-rest, which includes dry areas. The domain is $[0, 4] \times [0, 2]$. The bottom topography is given by

$$b(x, y) = \begin{cases} 1 - 0.8e^{-r}, & r := 2(x-2)^2 + 4(y-1)^2 < \log\left(\frac{8}{5}\right), \\ 0.8e^{-r}, & \text{otherwise}, \end{cases} \tag{6.2}$$

and the initial data are

$$u(x, y, t = 0) = v(x, y, t = 0) = 0, \quad h(x, y, t = 0) = \begin{cases} \max(0.45 - b(x, y), 0), & r < \log(\frac{8}{5}), \\ \max(0.3 - b(x, y), 0), & \text{otherwise}. \end{cases} \tag{6.3}$$

The simulation is done on 200×100 uniform cells until final time $t = 0.15$ (see Fig. 2). The steady states are preserved up to machine error. In Fig. 3 we mark those cells where the corrected reconstruction step developed in Section 2.3 is applied. The dry area is located between the elliptical fronts. In the right figure we see that the correction is applied both at the wet side and at the dry side of the wet-dry front.

6.3. Bottom reflections

In this section we show examples where the $\text{HR2}_{\text{ABBKP}}$ and the HR2_{BHNW} schemes may cause non-physical reflections. We begin with a number of one-dimensional Riemann problems in Section 6.3.1, and conclude with two-dimensional dam break problems in Section 6.3.2.

6.3.1. One-dimensional Riemann problems

We have tested the three schemes on seven Riemann problems [31,34–36] with $x \in [-1, 1]$ and with data (h_L, u_L, b_L) respectively (h_R, u_R, b_R) given in Table 3. All simulations are done until $t = 0.1$ on 1000 uniform cells. Since the bottom is discontinuous, we compute the reference solution by a careful limit process based on the recent analysis in [35,37] which we detail in Appendix A. In the right columns of Table 3 we note whether the schemes produce unphysical reflections. To make the figure legends readable, we write ABBKP instead of $\text{HR2}_{\text{ABBKP}}$, and BHNW instead of HR2_{BHNW}.

In Fig. 4 we display solutions of Riemann problems RP4 and RP5. The initial data of RP4 are fully wet. Therefore, the corrected reconstructions of the HR2_{BHNW} and BSGM scheme are not activated, and all three solutions coincide.

On the other hand for RP5, the $\text{HR2}_{\text{ABBKP}}$ and HR2_{BHNW} solutions exhibit a non-physical reflection originating at the origin, which is a partially wet point. To understand this reflection, we show the bottom reconstructions of the three schemes in Fig. 5.

6.3.2. Dam break over wet terrain

To highlight the issue of non-physical reflections, we consider two dam break problems over two-dimensional, discontinuous terrain. The domain is $(0, 300) \times (0, 200)$, a dam of height $b(x, y) = 20$ is located at $(85, 95) \times (0, 95)$ and $(85, 95) \times (170, 200)$, and in the remaining region, we initialize bottom and water depth by

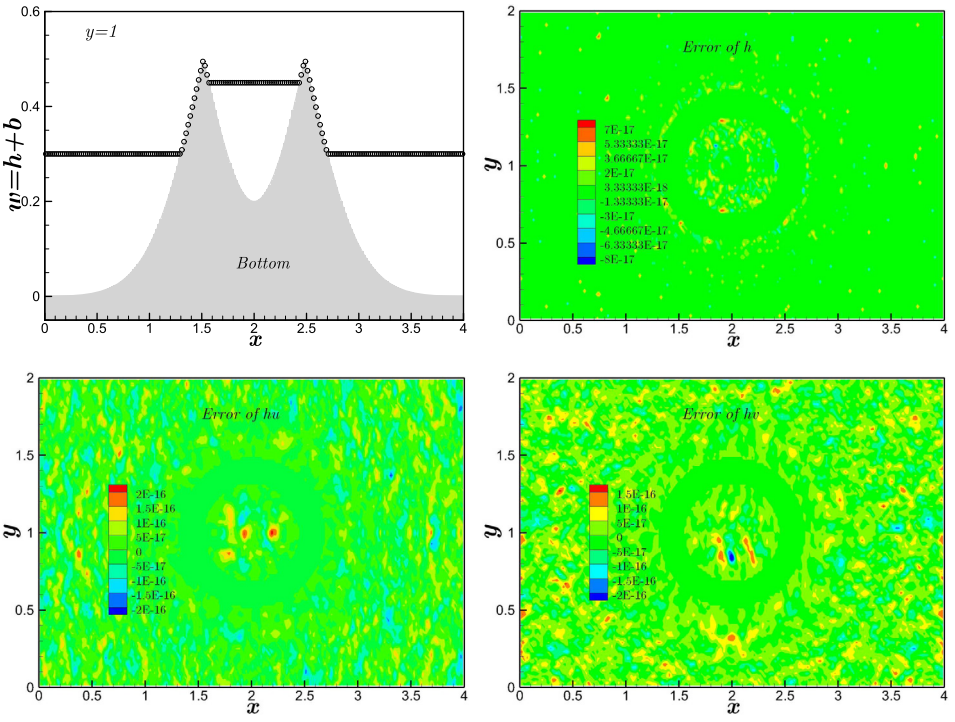

Fig. 2. BSGM scheme: two-dimensional well balanced test. 1-D slice (along y = 1) of the simulated result, and numerical errors of h, hu and hv. The simulation is done on 200×100 cells.

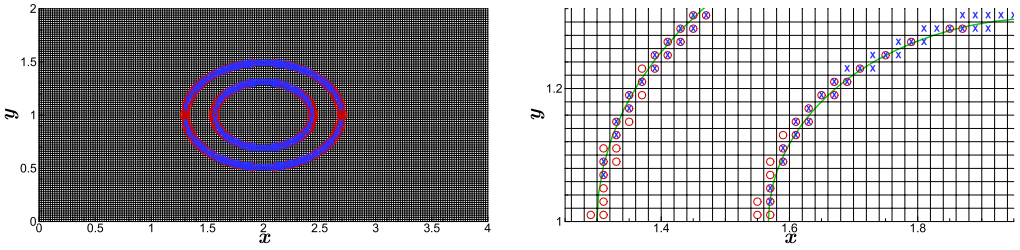

Fig. 3. BSGM scheme: two-dimensional well balanced test. Indicator where corrected reconstruction step is applied in x- direction (red circles) and y-direction (blue crosses), see Section 2.3. Full 200×100 grid (left) and detail (right).

Table 3
Riemann problems. The initial left and right states with bottom jumps. $\text{HR2}_{\text{ABBKP}}$ creates reflections in RP5 - RP7, and HR2_{BHNW} in RP5.

RP	h_L	h_R	u_L	u_R	b_L	b_R	$\text{HR2}_{\text{ABBKP}}$	HR2_{BHNW}	BSGM
1	4.0	0.50537954	0.1	0.0	0.0	1.5	ok	ok	ok
2	1.5	0.16664757	2.0	0.0	0.0	2.0	ok	ok	ok
3	0.3	0.4	2.0	2.2	1.1	1.0	ok	ok	ok
4	1.0	0.8	2.0	4.0	1.1	1.0	ok	ok	ok
5	0.75	1.0	0.0	0.0	1.0	0.0	REFL	REFL	ok
6	0.1	0.05	0.1	0.4	0.1	0.0	REFL	ok	ok
7	1.0	1.0	2.0	4.0	1.0	0.0	REFL	ok	ok

$$(b(x, y), h(x, y, t = 0)) = \begin{cases} (10, 7.5) & x < 90, \\ (0, 10) & x > 90. \end{cases} \tag{6.4}$$

The initial velocity is set to zero. We impose an outflow boundary condition at $y = 200$, and reflective boundary conditions at all other boundaries.

After the dam breaks, a shock wave propagates to the right, a rarefaction to the left, and a stationary shock is formed at the step. At later times, these waves interact with waves which are diffracted from the corners of the wall. In Fig. 6, the numerical results for $\text{HR2}_{\text{ABBKP}}$, HR2_{BHNW} and BSGM on 600×400 cells are displayed at times $t = 3$, $t = 6$ and $t = 9$.

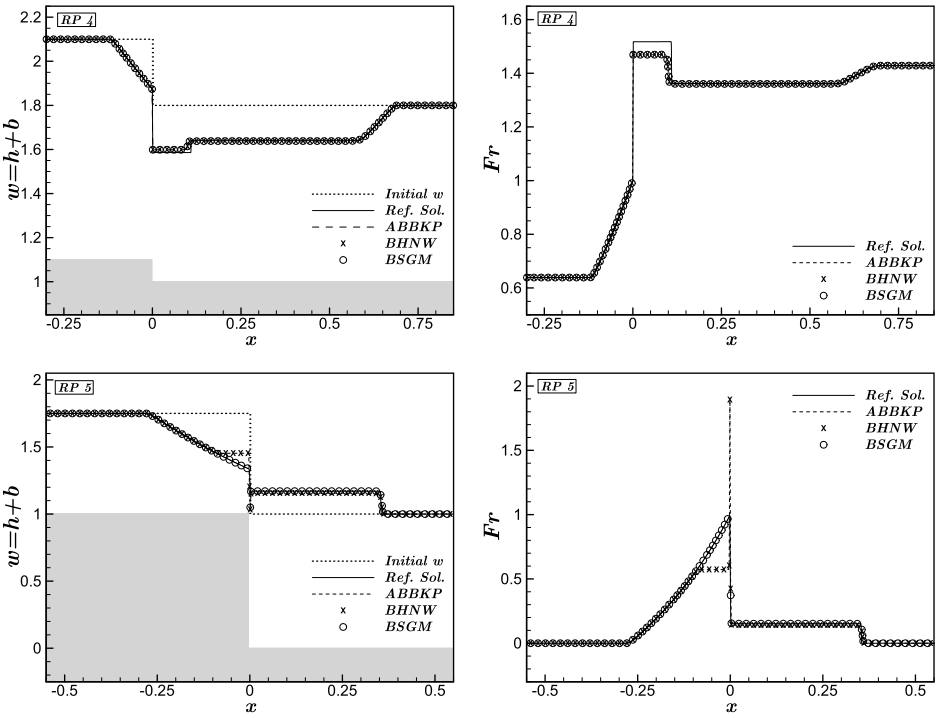

Fig. 4. Riemann Problems 4 (top row) and 5 (bottom row). Comparison of $\text{HR2}_{\text{ABBKP}}$, HR2_{BHNW} and BSGM schemes. For RP4 the three methods produce identical results and capture the wave patterns. For RP5, the $\text{HR2}_{\text{ABBKP}}$ and HR2_{BHNW} schemes produce identical results which contain a nonphysical reflection. This is cured by the BSGM.

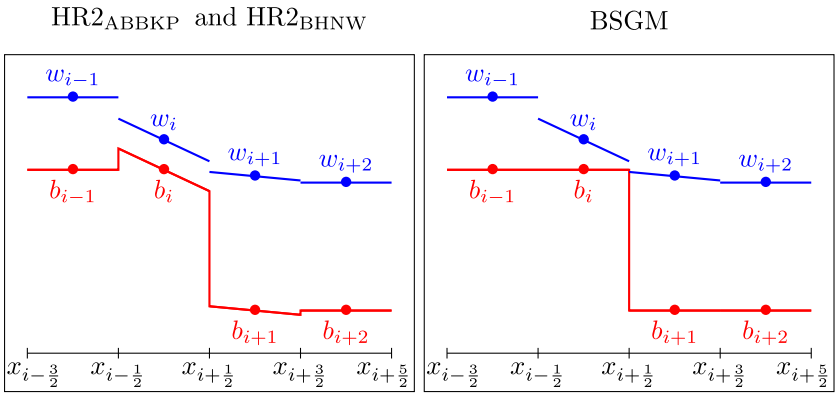

Fig. 5. Reconstruction for RP5. The $\text{HR2}_{\text{ABBKP}}$ and HR2_{BHNW} schemes create unphysical local extrema in the bottom. The BSGM gives a MMP bottom reconstruction.

The reference solution is computed on 2400×1600 cells, with an additional layer of 8 cells where the bottom is smoothed (see Appendix A for details). We plot 60 contours of the water surface, as well as two cross-sections along $y = 132.5$ and $y = 167.2$. Similarly to Riemann Problem RP5 in Fig. 4, the $\text{HR2}_{\text{ABBKP}}$ and HR2_{BHNW} schemes produce non-physical backward waves to the left of the step. Upon interacting with the waves diffracted from the corners of the wall, the schemes cannot recover the wave structure in the centre and to the left of the dam break. Clearly, the result by BSGM is converging to the reference solution.

6.3.3. Dam break over dry terrain

As our last example, we compute a dam break over dry terrain. The only difference to the initial data (6.4) is that $h(x, y, t = 0) = 0$ for $x > 90$. The numerical results are shown in Fig. 7. Once more, the $\text{HR2}_{\text{ABBKP}}$ produces a non-physical reflection. For this problem, both the HR2_{BHNW} and the BSGM schemes are reflection-free. While all three schemes preserve the positivity near the wet-dry front travelling to the right, the front position of the $\text{HR2}_{\text{ABBKP}}$ scheme seems to be slightly lagging behind.

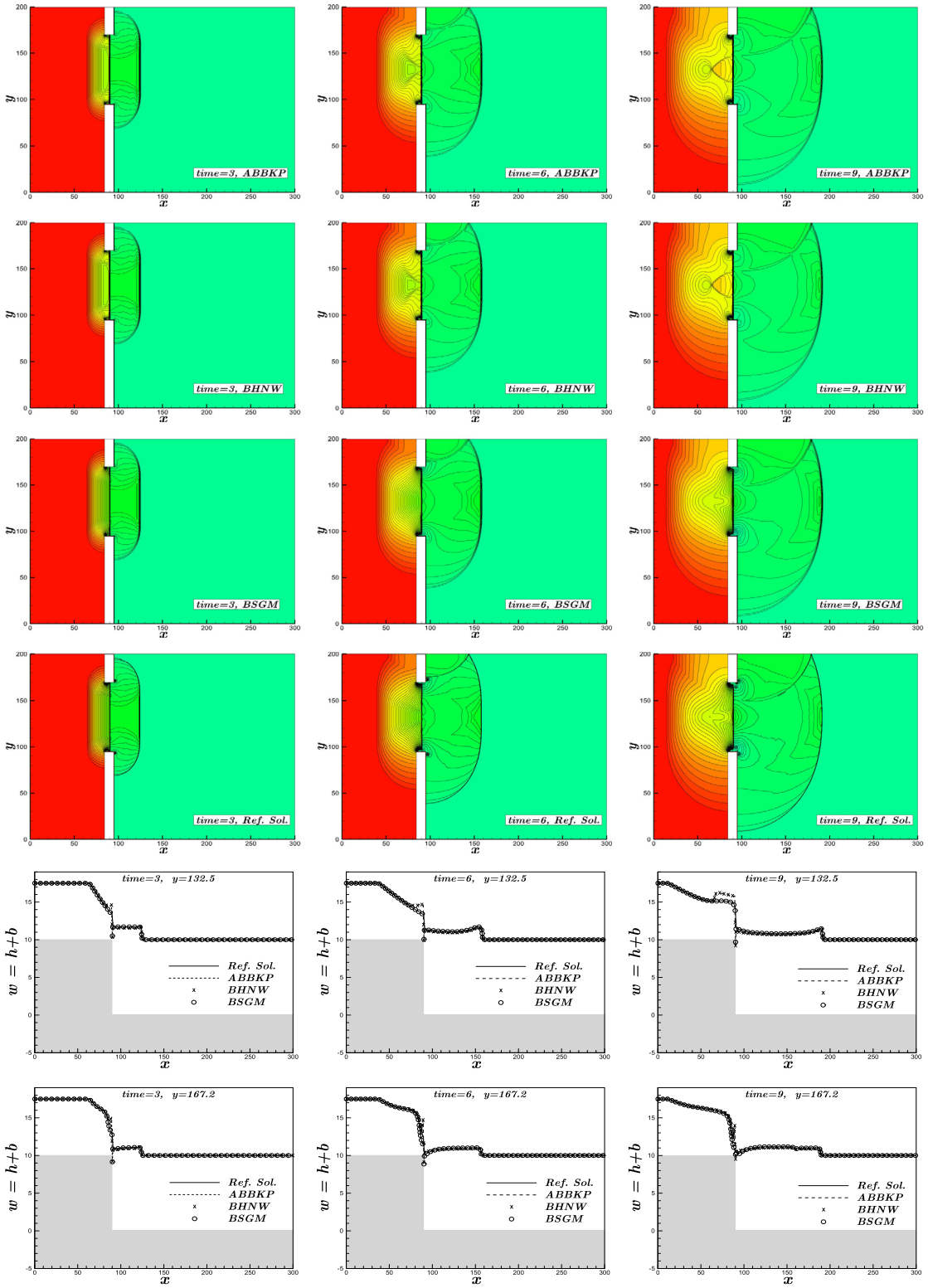

Fig. 6. Water surface levels for the two-dimensional dam break problem over wet terrain. Top to bottom: $\mathrm{HR2}_{\mathrm{ABBKP}}$, $\mathrm{HR2}_{\mathrm{BHNW}}$, BSGM, reference solution and cross sections at $y = 132.5$ and $y = 167.2$. Note the non-physical reflections of $\mathrm{HR2}_{\mathrm{ABBKP}}$ and $\mathrm{HR2}_{\mathrm{BHNW}}$ to the left of the step, which grow with time.

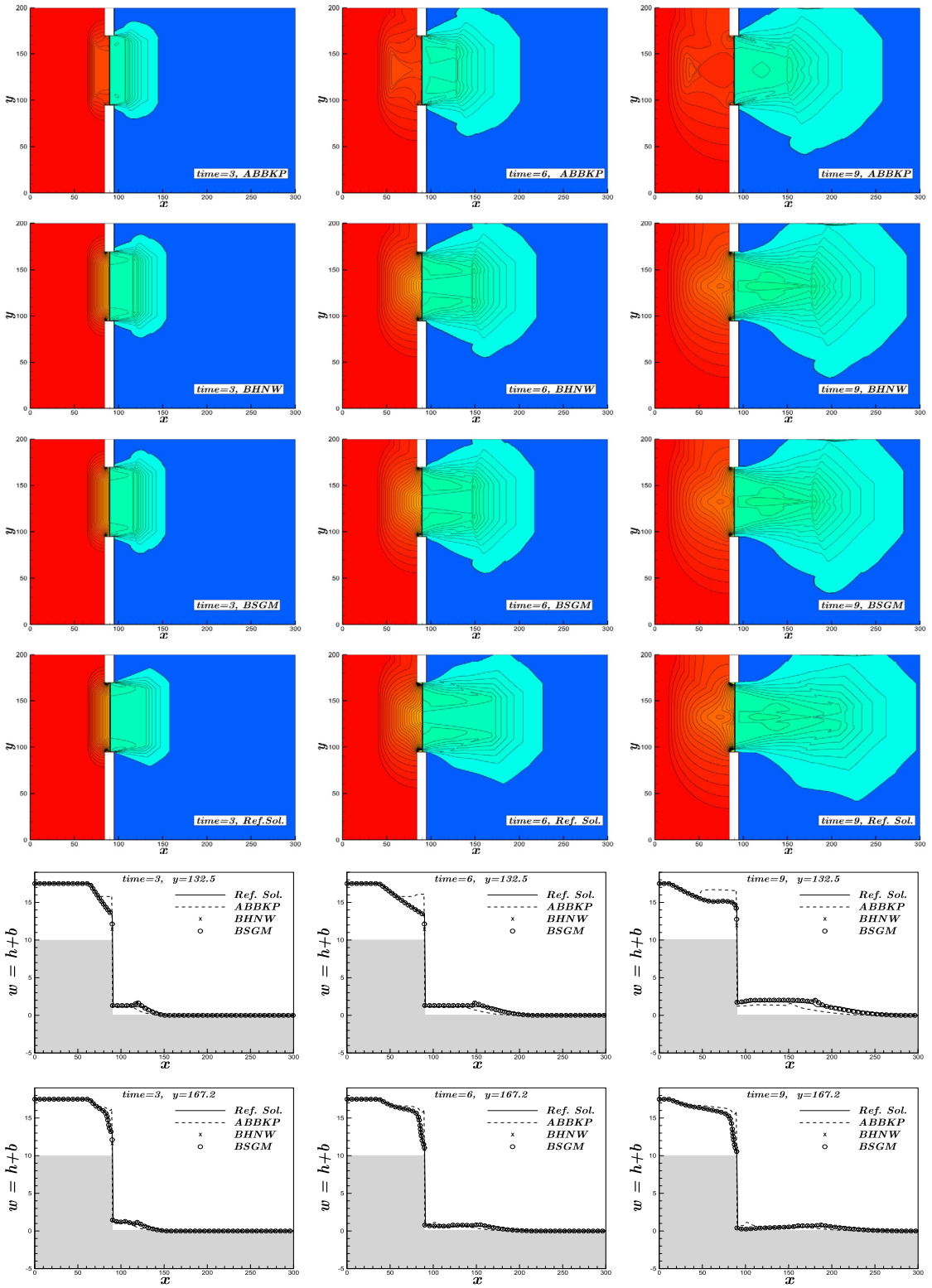

Fig. 7. Analogous to Fig. 6, but with dry bottom to the right of the step.

7. Conclusion

In this paper, we have revisited the key issues of well-balancing, positivity, and continuous versus discontinuous discretization of the bottom topography. The new bottom-surface-gradient reconstruction starts from a prescribed, piecewise linear, continuous or discontinuous reconstruction of the topography, which is modified only in exceptional cases to preserve positivity of the water height as well as the maximum-minimum-preserving property (MMP) for both b and $w = h + b$. For possible bottom discontinuities we apply the subcell hydrostatic reconstruction method to obtain a well-balanced, positivity preserving and second-order-accurate scheme. Numerical experiments in one and two space dimension give excellent results. In particular, they demonstrate that the BSGM scheme does not produce unphysical reflections near bottom steps.

CRediT authorship contribution statement

Guoxian Chen and **Sebastian Noelle** made equal contributions on theory, numerical experiments and writing.

Declaration of competing interest

The authors declare that they have no known competing financial interests or personal relationships that could have appeared to influence the work reported in this paper.

Acknowledgements

This work was supported in part by the National Science Foundation of China (11371023) and by the Deutsche Forschungsgemeinschaft under DFG grant 320021702/GRK2326. The authors would like to thank Sophie Hörnschemeyer for a careful reading and discussions of the manuscript.

Appendix A. Reference solution for discontinuous topography

When the prescribed bottom is continuous, we compute the reference solution by the $\mathrm{HR1}_{\mathrm{CN}}$ scheme on sufficiently refined grids. For discontinuous bottom the solution of the Riemann problem can be non-unique (see e.g. [35,34] and the references therein). A key difficulty is the possible coincidence of stationary waves, which is called resonance. Aleksyuk and Belikov [37] single out a unique resonant solution by demanding that the discharge hu at $x = 0$ should depend continuously on the initial conditions. They construct this solution by approximating the bottom with a sequence of monotone functions.

We follow this approach and approximate the topography linearly in a transition layer $(-\delta, \delta)$. Then we pass δ to zero numerically. At the same time, we increase the number of grid points in the transition layer. We denote the approximate solution for fixed $\delta > 0$ by U_δ and check numerically that

$$\|U_\delta\|_{L^\infty([-\delta,\delta])} \tag{A.1}$$

is uniformly bounded with respect to δ. This is evidence that the reference solution

$$U_{\mathrm{ref}} := \lim_{\delta \to 0} U_\delta \tag{A.2}$$

is absolutely continuous with respect to Lebesgue measure. As a consequence, we do not display U_δ in the transition layer, which has Lebuesgue measure zero in the limit. Finally, we control that the discharge $(hu)_{\mathrm{ref}}$ is continuous at $x = 0$.

References

[1] Saint-Venant, Théorie du mouvement non-permanent des eaux avec application aux crues des rivières et à l'introduction des marées dans leur lit, C. R. Hebd. Séances Acad. Sci. 73 (1871) 147–154.
[2] J.-F. Gerbeau, B. Perthame, Derivation of viscous Saint-Venant system for laminar shallow water; numerical validation, Discrete Contin. Dyn. Syst., Ser. B 1 (2001) 89–102.
[3] F. Alcrudo, P. García-Navarro, A high-resolution Godunov-type scheme in finite volumes for the 2d shallow-water equations, Int. J. Numer. Methods Fluids 16 (1993) 489–505.
[4] J.M. Greenberg, A.Y. Leroux, A well-balanced scheme for the numerical processing of source terms in hyperbolic equations, SIAM J. Numer. Anal. 33 (1) (1996) 1–16.
[5] S. Jin, A steady-state capturing method for hyperbolic systems with geometrical source terms, Math. Model. Numer. Anal. 35 (2001) 631–645.
[6] J.G. Zhou, D.M. Causon, C.G. Mingham, D.M. Ingram, The surface gradient method for the treatment of source terms in the shallow-water equations, J. Comput. Phys. 168 (1) (2001) 1–25.
[7] A. Kurganov, D. Levy, Central-upwind schemes for the Saint-Venant system, ESAIM: Math. Model. Numer. Anal. 36 (2002) 397–425.
[8] D.S. Bale, R.J. Leveque, S. Mitran, J.A. Rossmanith, A wave propagation method for conservation laws and balance laws with spatially varying flux functions, SIAM J. Sci. Comput. 24 (2002) 955–978.
[9] E. Audusse, F. Bouchut, M.-O. Bristeau, R. Klein, B. Perthame, A fast and stable well-balanced scheme with hydrostatic reconstruction for shallow water flows, SIAM J. Sci. Comput. 25 (2004) 2050–2065.
[10] M. Castro, J.M. Gallardo, C. Parés, High order finite volume schemes based on reconstruction of states for solving hyperbolic systems with nonconservative products. Applications to shallow-water systems, Math. Comput. 75 (2006) 1103–1134.

[11] S. Noelle, N. Pankratz, G. Puppo, J.R. Natvig, Well-balanced finite volume schemes of arbitrary order of accuracy for shallow water flows, J. Comput. Phys. 213 (2) (2006) 474–499.
[12] S. Noelle, Y. Xing, C.-W. Shu, High-order well-balanced finite volume WENO schemes for shallow water equation with moving water, J. Comput. Phys. 226 (1) (2007) 29–58.
[13] A. Kurganov, G. Petrova, A second-order well-balanced positivity preserving central-upwind scheme for the Saint-Venant system, Commun. Math. Sci. 5 (1) (2007) 133–160.
[14] M. Lukáčová-Medvid'ová, S. Noelle, M. Kraft, Well-balanced finite volume evolution Galerkin methods for the shallow water equations, J. Comput. Phys. 221 (2007) 122–147.
[15] J.M. Gallardo, M. Castro, C. Parés, J.M. González-Vida, On a well-balanced high-order finite volume scheme for the shallow water equations with bottom topography and dry areas, J. Comput. Phys. 227 (1) (2007) 574–601.
[16] Q. Liang, F. Marche, Numerical resolution of well-balanced shallow water equations with complex source terms, Adv. Water Resour. 32 (6) (2009) 873–884.
[17] Y. Xing, X. Zhang, C.-W. Shu, Positivity-preserving high order well-balanced discontinuous Galerkin methods for the shallow water equations, Adv. Water Resour. 33 (2010) 1476–1493.
[18] Y. Xing, X. Zhang, Positivity-preserving well-balanced discontinuous Galerkin methods for the shallow water equations on unstructured triangular meshes, J. Sci. Comput. 57 (2013) 19–41.
[19] A. Bollermann, G. Chen, A. Kurganov, S. Noelle, A well-balanced reconstruction of wet/dry fronts for the shallow water equations, J. Sci. Comput. 56 (2) (2013) 267–290.
[20] G. Chen, S. Noelle, A new hydrostatic reconstruction scheme based on subcell reconstructions, SIAM J. Numer. Anal. 55 (2) (2017) 758–784.
[21] C. Berthon, A. Duran, F. Foucher, K. Saleh, J.D.D. Zabsonre, Improvement of the hydrostatic reconstruction scheme to get fully discrete entropy inequalities, J. Sci. Comput. 80 (2) (2019) 924–956.
[22] X. Liu, J. Albright, Y. Epshteyn, A. Kurganov, Well-balanced positivity preserving central-upwind scheme with a novel wet/dry reconstruction on triangular grids for the Saint-Venant system, J. Comput. Phys. 374 (2018) 213–236.
[23] C. Klingenberg, A. Kurganov, M. Zenk, Moving-water equilibria preserving HLL-type schemes for the shallow water equations, Commun. Math. Res. 36 (3) (2020) 247–271.
[24] J. Dong, D.F. Li, Exactly well-balanced positivity preserving nonstaggered central scheme for open-channel flows, Int. J. Numer. Methods Fluids 93 (1) (2021) 273–292.
[25] E.F. Toro, Shock-Capturing Methods for Free-Surface Shallow Flows, Wiley, 2001.
[26] F. Bouchut, Nonlinear Stability of Finite Volume Methods for Hyperbolic Conservation Laws and Well-Balanced Schemes for Sources, Springer, 2004.
[27] L. Gosse, Computing Qualitatively Correct Approximations of Balance Laws, SIMAI Springer Series, vol. 2, Springer, Milan, 2013.
[28] A. Kurganov, Finite-volume schemes for shallow-water equations, Acta Numer. 27 (2018) 289–351.
[29] G. Dal Maso, P.G. Lefloch, F. Murat, Definition and weak stability of nonconservative products, J. Math. Pures Appl. (9) 74 (6) (1995) 483–548.
[30] M.J. Castro, P.G. LeFloch, M.L. Muñoz Ruiz, C. Parés, Why many theories of shock waves are necessary: convergence error in formally path-consistent schemes, J. Comput. Phys. 227 (17) (2008) 8107–8129.
[31] A. Buttinger-Kreuzhuber, Z. Horváth, S. Noelle, G. Blöschl, J. Waser, A fast second-order shallow water scheme on two-dimensional structured grids over abrupt topography, Adv. Water Resour. 127 (2019) 89–108.
[32] G. Sigal, D. Ketcheson, C.-W. Shu, Strong Stability Preserving Runge-Kutta and Multistep Time Discretizations, World Scientific, Singapore, 2011.
[33] B. Einfeldt, C.D. Munz, P.L. Roe, B. Sjögreen, On Godunov-type methods near low densities, J. Comput. Phys. 92 (2) (1991) 273–295.
[34] E. Han, G. Warnecke, Exact Riemann solutions to shallow water equations, Q. Appl. Math. 72 (3) (2014) 407–453.
[35] P.G. LeFloch, M.D. Thanh, A Godunov-type method for the shallow water equations with discontinuous topography in the resonant regime, J. Comput. Phys. 230 (20) (2011) 7631–7660.
[36] J. Murillo, P. García-Navarro, Weak solutions for partial differential equations with source terms: application to the shallow water equations, J. Comput. Phys. 229 (2010) 4327–4368.
[37] A.I. Aleksyuk, V.V. Belikov, The uniqueness of the exact solution of the Riemann problem for the shallow water equations with discontinuous bottom, J. Comput. Phys. 390 (2019) 232–248.